Poly(ethylene oxide)-Poly(propylene oxide)-Poly(ethylene oxide) Triblock Copolymers in Aqueous Solution. The Influence of Relative Block Size

Kell Mortensen*

Physics Department, Risø National Laboratory, DK-4000 Roskilde, Denmark

Wyn Brown

Department of Physical Chemistry, University of Uppsala, S-75121 Uppsala, Sweden

Received February 16, 1993; Revised Manuscript Received April 19, 1993

ABSTRACT: The phase behavior of a series of poly(ethylene oxide)-poly(propylene oxide)-poly(ethylene oxide), $E_mP_nE_m$, triblock copolymers dissolved in water has been studied using small-angle neutron and dynamic light scattering. The block copolymers were chosen with a common polymerization degree of the central PPO block, $n = 39$, but different degrees of polymerization of the outer PEO blocks, m ranging from 6 to 97. All copolymers show the characteristics of fully dissolved polymers at low temperatures, whereas aggregates are formed at elevated temperatures due to the hydrophilic-to-hydrophobic transition in PPO. The scattering function of the $m = 27$-96 aggregates has been analyzed in terms of hard-sphere interacting micelles, characterized by a dense core radius R_c, and a hard-sphere interaction radius R_{hs}. It appears from the data analysis that the core size increases with decreasing degree of polymerization m and with increasing temperature. While the copolymer with the highest degree of polymerization m aggregates in micelles with a core diameter which, within the whole temperature regime, is smaller than the length of a stretched PPO-chain, the intermediate m copolymer micelles have a core diameter which at high temperature approaches the size of a fully stretched PPO chain, thus causing an abrupt departure from spherical to rodlike structure, as observed both by neutron scattering and depolarized light scattering. Extrapolating the information on the core diameter for the $m = 27$-96 copolymer micelles predicts for the $m = 6$ copolymer a core size which at all temperatures exceeds the length of the fully stretched PPO block, thus explaining the absence of micelle formation for this copolymer. It appears from the hard-sphere data analysis that the micelle-forming polymers can all be scaled to a common phase behavior where the critical micellation temperature is determined by the PPO concentration, whereas the crystallization temperature is determined by the total copolymer concentration.

I. Introduction

Block copolymers composed of poly(ethylene oxide), PEO or E_m, and poly(propylene oxide), PPO or P_n, have attracted increasing attention during the last few years.[1-14] This is partly due to their wide range of applications as nonionic surface-active agents and partly because of their unique behavior which is of fundamental interest in physics.[1,2]

The association properties of triblock copolymers $E_mP_nE_m$ in aqueous solutions have been studied by various techniques, and the thermally reversible gelation, displayed in some cases, has been the subject of many investigations. Recently it was shown by neutron scattering that the gel state is a crystalline phase of body-centered cubic (bcc) ordered spherical micelles.[1-3] Details of the association of $E_mP_nE_m$ unimers into aggregates have also been the subject of a number of investigations.[3-10]

Different $E_mP_nE_m$ triblock copolymers with varying m and n have been studied. In many cases there is association into micelles at elevated temperatures, but other forms of aggregates may also form. Our understanding of the role of the detailed molecular architecture, for example, the degree of polymerization, is incomplete however. Recently, Brown et al.[14] investigated a series of triblock copolymers $E_mP_nE_m$ with fixed $n = 39$ but m varying from 6 to 96, using dynamic light scattering and dynamic mechanical measurements. They found that, while the micellar form of aggregates is stable up to relatively high temperatures for the high PEO content copolymers, those having the lowest PEO content form a two-phase system dominated by large clusters. The copolymers with intermediate contents of PEO form micellar aggregates over a limited temperature range.[2,3,14]

Below, we present structural studies on the series of polymers described previously by Brown et al.[14] The aim is to achieve a better understanding of the role of the molecular architecture and more specifically to understand which physical parameters are crucial for association into a spherical micellar form, with subsequent formation of an ordered micellar crystal.

It has previously been shown that, in spite of the soft "corona" of flexible PEO chains, the $E_mP_nE_m$ micellar aggregates can, to a very good approximation, be treated as hard-sphere interacting objects.[1-3] The thermoreversible gel transition is easy to understand using this analysis as due to hard-sphere crystallization, when the micellar hard-sphere volume fraction approaches the critical value for crystallization. The volume fraction of 0.53 close to the gelation temperature is in excellent agreement with expectations from theoretical studies.[15] Below, we will use the hard-sphere interaction potential, together with the Percus-Yevick approximations to extract structural parameters from the neutron scattering data.

II. Experimental Section

A. Material. The triblock copolymer, poly(ethylene oxide)-poly(propylene oxide)-poly(ethylene oxide), $H[OCH_2CH_2]_m[OCH_2CH(CH_3)]_n[OCH_2CH_2]_mH$ or $E_mP_nE_m$, with $n = 39$, and $m = 6$, 67, and 96 abbreviated respectively L81, F87, and F88, were obtained from BASF Wyandotte Corp., NJ, whereas the $m = 39$, $n = 27$ polymer, abbreviated P85,[16] was obtained from Serva AG, Heidelberg, Germany. The triblock copolymers were used without further purification. The copolymers were

0024-9297/93/2226-4128$04.00/0

dissolved in water at 5 °C, at which temperature they form a transparent, homogeneous solution. Deuterated water, D_2O, was used in order to get good contrast and low background for the neutron scattering experiments. The solutions discussed below are all given in weight percent.

B. SANS. Small-angle neutron scattering experiments were performed using the Risø SANS facility, which is a flexible instrument covering scattering vectors from 0.002 to 0.5 Å^{-1}, with variable neutron wavelength resolution.

The samples were mounted in sealed quartz containers (Suprasil from Hellma, FRG), with a 2-mm flight path. For the neutron spectra of water, used for calibration, a 1-mm-thick quartz container was used.

The results presented below were obtained using neutrons with 6-Å wavelength, with sample-to-detector distances of 3 m, giving scattering vectors in the range 0.01–0.1 Å^{-1}, where the scattering vector **q** is given by the scattering angle θ and the neutron wavelength λ: $|\mathbf{q}| = q = (4\pi/\lambda)\sin(\theta/2)$. The neutron wavelength resolution used was $\Delta\lambda/\lambda = 0.18$, and the neutron beam collimation was determined by the pinhole sizes of 16- and 7-mm diameter at the source and sample positions, respectively, and collimation lengths of 3 m. The smearing induced by the wavelength spread, the collimation, and the detector resolution was included in the data analysis discussed below, using Gaussian approximations for the different terms.[17]

The scattering data were corrected for the background arising from the quartz container with D_2O and from other sources, as measured with the neutron beam blocked by plastic containing boron at the sample position. The incoherent scattering from H_2O was used to determine deviations from a uniform detector response and to convert the data into absolute units.

The scattering patterns discussed in the present paper are all azimuthally isotropic. The data have therefore been reduced to the one-dimensional $I(q)$ scattering functions which are only dependent on the absolute value of q.

C. Dynamic Light Scattering. Polarized dynamic light scattering (I_{VV}) measurements were made using the apparatus and techniques described earlier (see, for example, Nicolai et al.[23]). The data were assembled using a wide-band multi-τ-autocorrelator (ALV5000) allowing characterization of relaxation time distributions extending over 8 decades. Average diffusion coefficients were estimated using the method of cumulants, with both second- and third-order terms. For a system exhibiting a continuous distribution of relaxation times (τ), the field correlation function, $g_1(t)$, is described by the Laplace transform

$$g_1(t) = \int_0^\infty \tau A(\tau)\, e^{-t/\tau}\, d \ln \tau$$

Inverse Laplace transformation was made by a nonlinear least-squares residual fit to $g_1(t)$, employing the REPES algorithm.[24] The range of relaxation times allowed in the fitting was between 0.5 μs and 1 s with a density of 12 points per decade. The "smoothing" parameter used in the program was selected as 0.5 in all cases. Relaxation rates are obtained from the moments of the peaks in the resulting relaxation time distribution.

Mutual diffusion coefficients (calculated from the measured relaxation rate, $\Gamma = 1/\tau$, and scattering vector, q: $D = \Gamma/q^2$) and the relative amplitudes were obtained from the moments of the peaks and are given in the output of the REPES program.

Depolarized dynamic light scattering (I_{VH}) was used to determine the rotational diffusion coefficient. The polarized intensity was very low (of the magnitude 3 kHz corresponding to a ratio I_{VH}/I_{VV} of approximately 1.5%, with a laser power of 200 mW).

III. Results and Discussion

Figures 1–4 show some characteristic neutron scattering data for L81, P85, F87, and F88, as obtained at different temperatures. The scattering curves shown are for 9% polymer solutions, but qualitatively similar behavior was obtained over a wide range of concentrations, ranging from 1 to 35%.[3]

The scattering patterns all show the following typical characteristics: at low temperatures, the scattering function shows a relatively weak q-dependence and the absolute intensity is small. As the temperature increases, the intensity increases and the q-dependence becomes stronger, revealing aggregation of copolymers.

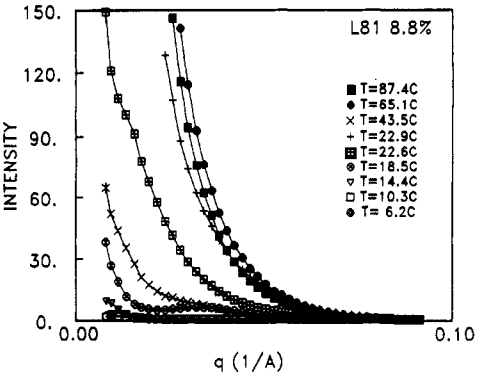

Figure 1. Scattering function I versus q for an aqueous solution of 9% $E_6P_{39}E_6$, L81 triblock copolymer, obtained in the 6–87 °C temperature range. (The solid lines connect data points.)

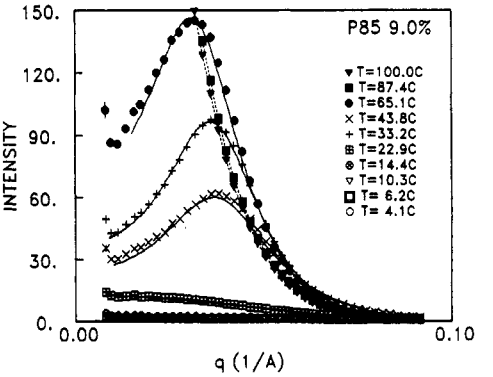

Figure 2. Scattering function I versus q for an aqueous solution of 9% $E_{27}P_{39}E_{27}$, P85 triblock copolymer, obtained in the 4-100 °C temperature range. The solid lines represent fits to the experimental data according to the hard-sphere Percus-Yevick model described in the text. The broken lines for the T>87 °C data are guides to the eye.

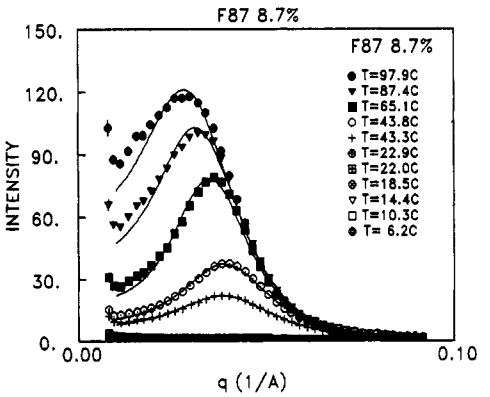

Figure 3. Scattering function I versus q for an aqueous solution of 9% $E_{67}P_{39}E_{67}$, F87 triblock copolymer, obtained in the 6–98 °C temperature range. The solid lines represent fits to the experimental data according to the hard-sphere Percus-Yevick model, described in the text.

At even higher temperatures, the scattering functions for the P85, F87, and F88 copolymer solutions are increasingly dominated by a pronounced peak, revealing important spatial correlation between neighboring aggregates. The correlation peak becomes significantly more pronounced at high copolymer concentrations. For copolymer concentrations beyond approximately 20%, a slight narrowing of the correlation peak is observed within limited temperature regimes due to long-range ordered

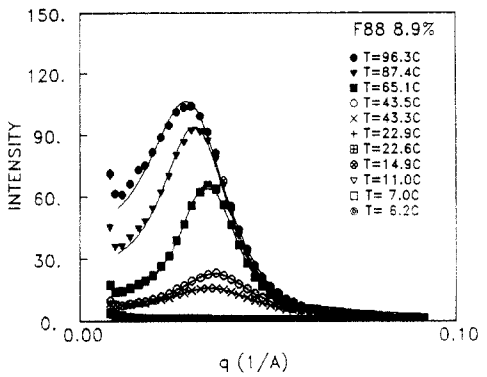

Figure 4. Scattering function I versus q for an aqueous solution of 9% $E_{96}P_{39}E_{96}$, F88 triblock copolymer, obtained in the 6–97 °C temperature range. The solid lines represent fits to the experimental data according to the hard-sphere Percus–Yevick model described in the text.

crystalline aggregates.[1,2] For temperatures above approximately 60 °C, the scattering function of P85 changes somewhat in character, as seen in Figure 2 showing an increasing intensity at the smallest scattering vectors, revealing changes in the micellar structure.[3] In the solutions of lower polymer concentration, the correlation peak completely vanishes within the same temperature regime. The F87 solutions show corresponding, although less pronounced, changes in the low-q scattering pattern at temperatures in the vicinity of 70 °C. The scattering pattern of F88 does not give rise to similar effects up to at least 90 °C, indicating that the F88 aggregates retain the same basic structure up to the highest temperatures.

The L81 polymer solutions show characteristics quite different from those of P85, F87, and F88. At low temperatures, L81 also shows only low scattering intensities, as expected for fully dissolved copolymer molecules. However, as the temperature is increased, the scattering function becomes very intense compared to the other three copolymer solutions of the same concentration, and with a much more steep q-dependence, indicating large, loosely connected aggregates. A correlation peak is observed only over a rather narrow temperature regime, and this peak is superimposed on an increasing small-angle term (cf. the 18 °C spectrum shown in Figure 1). Moreover, while the P85, F87, and F88 copolymers form one-phase solutions over the whole temperature range studied, i.e., 5–90 °C, L81 exhibits macroscopic phase separation and forms a two-phase system at temperatures above approximately 15 °C. The scattering pattern shown in Figure 4 is dominated by the lower phase. More studies are needed for a detailed discussion of the L81 aggregates. This will be the subject of a forthcoming report.

A. Gaussian Unimers. The low-temperature neutron scattering patterns of relative small intensity have previously been shown to be consistent with fully dissolved Gaussian copolymer molecules.[3] For P85, we found a radius of gyration equal to 17 Å. The L81, F87, and F88 suspensions give scattering curves which imply radii of gyration of the same order of magnitude, but measurements over extended q-ranges are needed for more precise values for the latter copolymers. For comparison, the hydrodynamic radii obtained from dynamic light scattering are 15, 18, 27, and 29 Å for respectively L81, P85, F87, and F88.[11,14] Investigations on the copolymer radius of gyration are interesting in themselves, and it is important to look for possible conformational changes close to the critical micellation temperature. Our studies up to now have not been able to reveal such effects.

B. Micellar Aggregates. At temperatures close to ambient, the poly(propylene oxide) part of the polymer chain is no longer soluble in water.[25] The resulting amphiphilic character of $E_mP_nE_m$ triblock copolymers leads to the formation of various aggregates, depending on the degree of polymerization of the blocks. A detailed neutron scattering study on the P85 solutions showed that these $E_mP_nE_m$ aggregates have the form of spherical micelles over a wide temperature regime;[2,3] i.e., the aggregates have the form of a core presumably dominated by propylene oxide blocks and which is surrounded by a corona of hydrated ethylene oxide subchains. Neutron scattering studies over a limited concentration range of F88 have already shown that F88 also aggregates in the form of micelles.[1]

The similarities between the results for P85, F87, and F88, as expressed in Figures 2–4, strongly indicate that the structural phase behavior of these polymers is to a large extent of the same type; i.e., the aggregates are dominated by spherical micelles over wide temperature ranges. This is supported by the dynamic light scattering studies already published.[8,14]

As the temperature, or the concentration, is increased, the scattering function becomes increasingly dominated by a pronounced correlation peak which reveals significant interactions between neighboring micelles (cf. Figures 2–4). In the high-q range well beyond the correlation peak, on the other hand, the scattering function remains effectively unchanged, indicating that the changes in the observed scattering pattern primarily reflect the increasing number density of the micelles, wheresas the characteristic form of the individual micelles is relatively unaffected by increasing the temperature or the concentration.

In dilute suspensions, where no interference occurs between scattering from different particles, the scattering function is given by the form factor $P(q)$. In more dense suspension interference significantly affects the scattering function. For a monodisperse system of particles, the scattering function can be written as the product of the single-particle form factor and the structure factor, $S(q)$, describing these interparticle interferences:[19]

$$I(q) = \Delta\rho^2 n' V^2 P(q)\, S(q) \qquad (1)$$

where $\Delta\rho^2$ is the contrast factor and n' is the number density of scatterers of volume V. Although it is clear from the absence of oscillations and the absence of an approaching $I \propto q^{-4}$ relationship that the micelles do not have a sharp surface,[3] we will as a first approach analyze the data in terms of dense spheres, using the form factor

$$P(q) = \left[\frac{3}{(qR_c)^3}(\sin(qR_c) - qR_c\cos(qR_c))\right]^2 \qquad (2)$$

characterized by the radius R_c, which is attributed to the size of the micellar core. The experimental deviations from eq 2 can be a result of the PEO subchains dispersed into the water phase, in agreement with a simplified model of the micellar structure with a central, dense core of predominantly poly(propylene oxide) and an outer corona of hydrated poly(ethylene oxide) effectively grafted onto the surface of the core, as previously discussed.[3] Deviation from the exact spherical form will also change the high-q behavior. Recent numerical studies on micellar aggregation have shown pronounced deviation from the classical spherical micellar form.[18]

The structure factor, $S(q)$, is given by the radial distribution function, $g(R)$, describing the arrangement

of the micelles:[19]

$$S(q) = 1 + 4\pi n' \int (g(R) - 1)\frac{\sin(qR)}{qR} R^2 \, dR \qquad (3)$$

Using the classical Ornstein–Zernike approximation for the spatial correlation fluctuations and the Percus-Yevick approximation for describing the direct correlation between two scattering objects[20] with a *hard-sphere* nearest-neighbor interaction potential, the structure factor can be written in the analytical form[3,21,22]

$$S(q) = \frac{1}{1 + 24\phi G(2qR_{hs}, \phi)/(2qR_{hs})} \qquad (4)$$

where G is a trigonometric function of the hard-sphere interaction radius R_{hs} and the hard-sphere volume fraction, ϕ. Thus, by least-squares residual fitting routines the experimental scattering function can be analyzed in terms of three parameters characterizing the micellar aggregates: the core radius R_c dominating the form factor $P(q)$ and the hard-sphere interaction parameters R_{hs} and ϕ.

Figures 2–4 include the scattering function, eqs 1–4, fitted to data for F88, F87, and P85 solutions. The fits are all very good, within the q-range discussed.

Figures 5–11 show the parameters resulting from the hard-sphere data analysis. The P85 data have already been published in refs 3 and 13, and the high concentration data for F88 have been reported previously in refs 1 and 12. Above approximately 60 °C, somewhat dependent on concentration, the P85 scattering functions no longer give good fits using the hard-sphere model. This is because of a spherical-to-prolate transformation in the micellar form, as previously shown.[3] The resulting parameters of the F87 suspensions suggest a similar conformational change in the micellar structure in the $T \sim 70$ °C temperature range, and for F88 a change may occur at $T \sim 90$–95 °C. Also, in the ordered gel phase, the hard-sphere model should give rise to some systematic errors, as the crystalline order causes correlations beyond the liquid nearest-neighbor interaction. However, as was shown in ref 1, the bond-length correlations remain basically liquidlike even in the *cubatic* ordered phase. Systematic errors in the resulting parameters should therefore be small, and the use of the Percus–Yevick hard-sphere approximation is accordingly validated.

Figure 5 shows the hard-sphere volume fraction ϕ plotted versus temperature for different concentrations of P85, F87, and F88. The three copolymers show quite similar behavior. At low temperatures, the micellar volume fraction approaches zero, indicating that all copolymers are dissolved as individual unimers. Above a critical micellation temperature (T_{cm1}), the volume fraction appears roughly linear in temperature until a saturated value, ϕ_0, is reached at T_{cm2}.

Within the temperature range T_{cm1}–T_{cm2}, micelles are in thermodynamic equilibrium with the unimers,

$$\text{unimers} \rightleftharpoons \text{micelles} \qquad (5)$$

The approximately linear correlation between temperature (T–T_{cm1}) and micellar concentration, ϕ, shows that the equilibrium constants have rather simple temperature dependencies.[3] Above the upper critical temperature, T_{cm2}, unimers are probably still present, but in a very small number density.[3]

As pointed out in ref 3, it is interesting to note that to a good approximation the limiting volume fraction, ϕ_0, increases linearly with polymer concentration, C, as shown in Figure 6. This is in agreement with expectations if the limiting micelle concentration corresponds to the situation where all unimers have aggregated into micelles, i.e.

$$\phi_0 = C/N(4\pi R_{hs}^3/3V_{EPE}) \qquad (6)$$

where N is the aggregation number, $(4/3)\pi R_{hs}^3$ is the hard-sphere micellar volume, and $V_{EPE} = 2mV_E + nV_P$ is the dry polymer volume, with V_E and V_P the molecular volumes

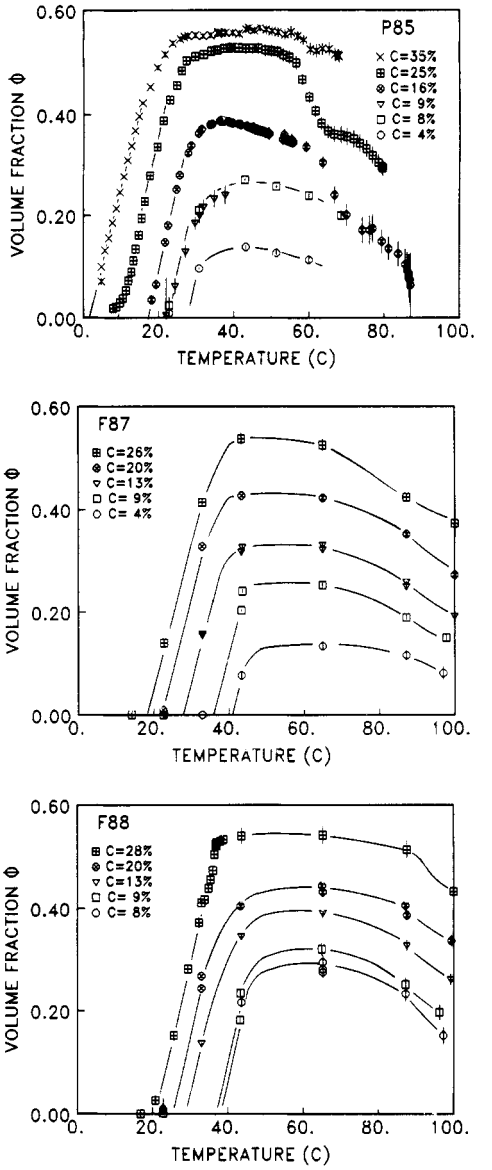

Figure 5. Resulting micellar hard-sphere volume fraction ϕ for aqueous solutions of $E_mP_nE_m$, $n = 39$, and $m = 27$ (P85), $m = 67$ (F87), and $m = 96$ (F88), obtained by fitting the hard-sphere Percus–Yevick model to the scattering data.

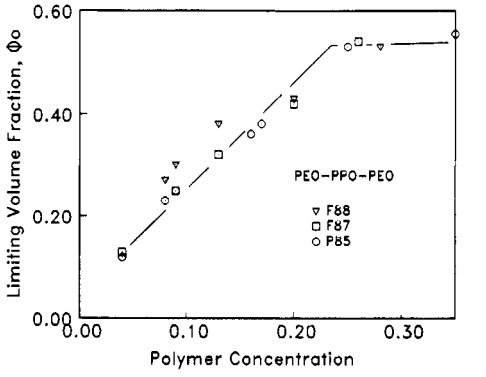

Figure 6. Copolymer concentration dependence of the limiting micellar volume fraction ϕ_0 as obtained at 50 °C from the data for P85, F87, and F88 presented in Figure 5. The limiting value of ϕ_0 at $\phi_c = 0.53$ is given by the hard-sphere crystallization value.

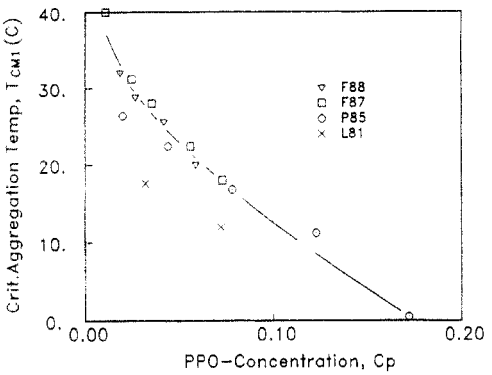

Figure 7. Critical aggregation temperature plotted versus concentration of PPO C_P. The P85, F87, and F88 data represent the critical micellation temperature T_{cm1} as obtained from the data presented in Figure 5. The L81 data are calculated from the onset of a dramatic increase in the integrated scattering intensity.

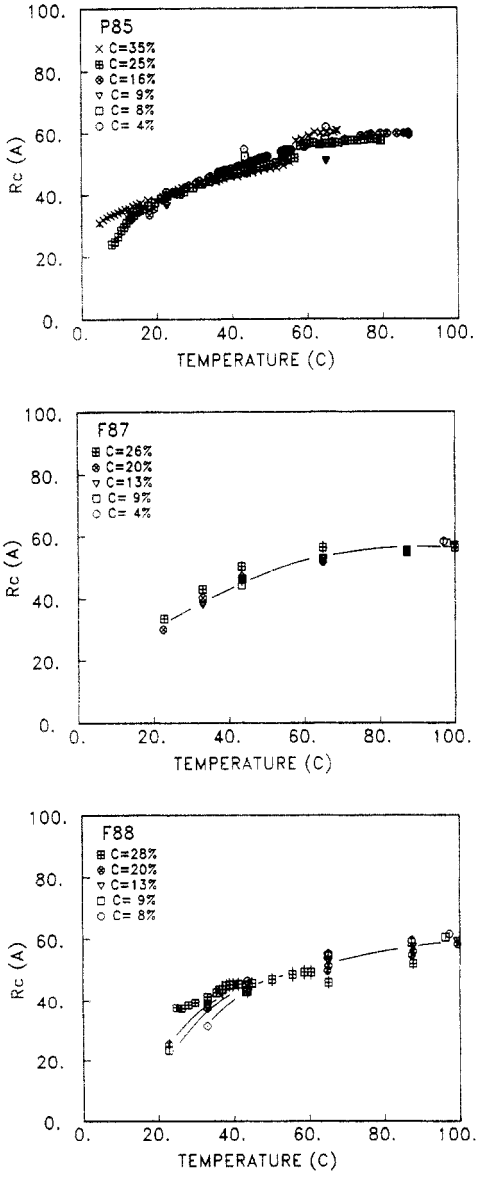

Figure 8. Resulting core radius R_c for aqueous solutions of $E_mP_nE_m$, n = 39, and m = 27 (P85), m = 67 (F87), and m = 96 (F88), obtained from the form factor in fitting the hard-sphere Percus–Yevick model to the scattering data.

of EO and PO monomers, respectively. It appears from Figure 5 that, for polymer concentrations below approximately 20%, there is a small temperature dependence of

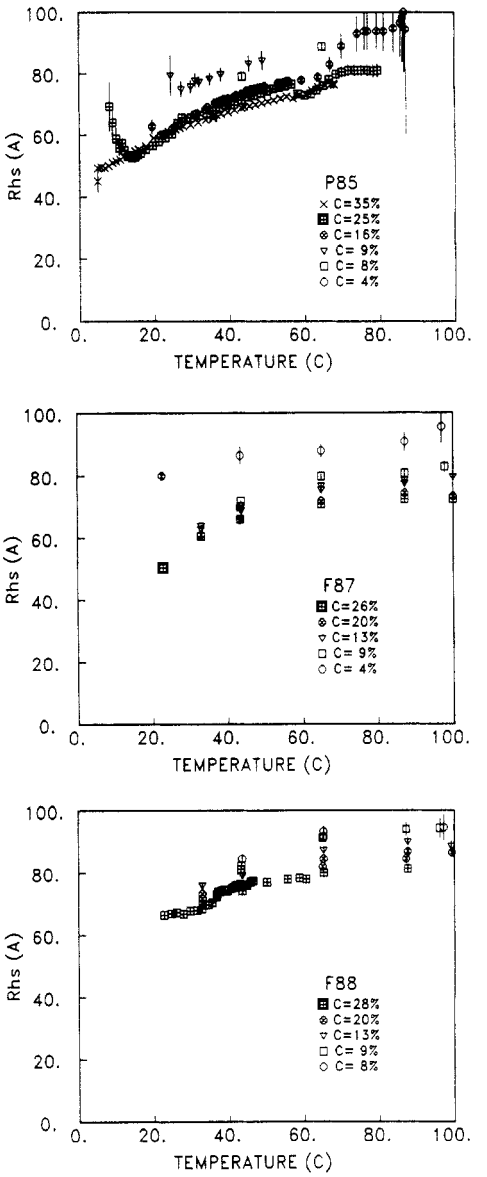

Figure 9. Resulting hard-sphere interaction radius R_{hs} of aqueous solutions of $E_mP_nE_m$, n = 39, and m = 27 (P85), m = 67 (F87), and m = 96 (F88), as obtained by fitting the hard-sphere Percus–Yevick model to the scattering data.

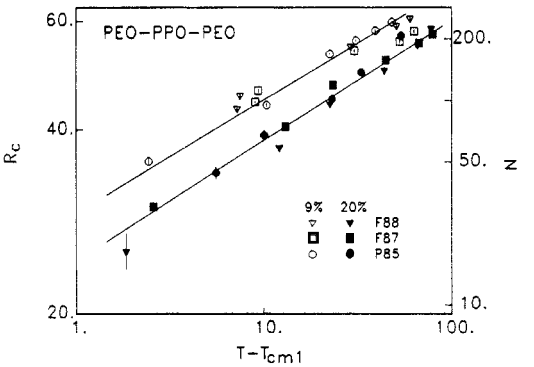

Figure 10. Resulting core radius R_c of 9% and 20% aqueous solutions of $E_mP_nE_m$, n = 39, and m = 27 (P85), m = 67 (F87), and m = 96 (F88), as presented in a double-logarithmic plot of R_c versus reduced temperature, revealing power law behavior.

the saturation value ϕ_0. This reflects changes in the micellar size, and thereby aggregation number, as will be more evident in the discussion of R_c and R_{hs} below. The ϕ_0 data shown in Figure 6 were obtained at T = 50 °C. The crossover from a linear increase in ϕ_0 with temperature to saturation at ϕ_c = 0.53 reflects the hard-sphere crystal-

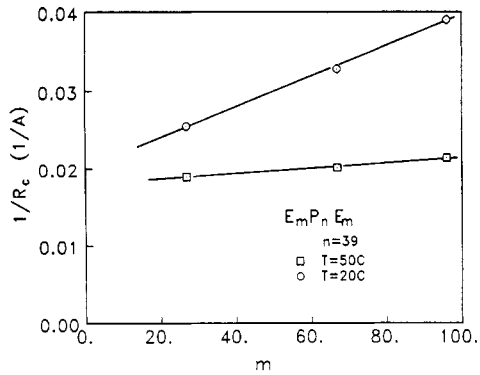

Figure 11. Core radius R_c of a 20% aqueous solution of $E_mP_nE_m$, $n = 39$, and $m = 27$ (P85), $m = 67$ (F87), and $m = 96$ (F88), as presented as $1/R_c$ versus degree of PEO polymerization m.

lization transition, previously discussed for F88[1] and P85.[2] For a polymer concentration above ~20% the limiting micellar volume fraction remains at this critical hard-sphere crystallization value, independent of changes in micellar sizes. The rather similar ϕ_0 versus C behavior for P85, F87, and F88 indicates that all three copolymers crystallize within the same concentration range (roughly 18–22%). It appears from Figure 5, however, that the characteristic temperatures for micelle formation and crystallization are significantly lower for the low m copolymer P85 than for the two other copolymers with larger m's, F87 and F88.

Figure 6 indicates, moreover, that the relevant polymer concentration in connection with the order-to-disorder transition is the total polymer concentration C, rather than the specific concentration of PPO blocks C_P.

Figure 7 shows the critical micellization temperature plotted versus the concentration of poly(propylene oxide), as given by the polymer concentration: $C_p = CnM_P/(nM_P + 2mM_E)$, where $M_P = 58$ and $M_E = 44$ are the molecular masses of respectively propylene oxide and ethylene oxide. Although the data are dominated by significant scattering due to statistical errors, it clearly appears that the PPO concentration is the relevant parameter decisive for determination of the micellization temperature. Figure 7 also includes the critical temperature for aggregate formation in L81. It is seen that L81 forms aggregates at temperatures below the common curve for the critical micellization temperature, presumably due to the much more hydrophobic nature of L81.

Figures 8 and 9 show respectively the core radius R_c and the hard-sphere interaction radius R_{hs}, obtained by least-squares fitting to the experimental scattering data. The radii are plotted versus temperature for different copolymer concentrations. The micellar core radius, R_c, and to some extent also the hard-sphere radius, R_{hs}, appear to be essentially independent of polymer concentration but show a significant increase with increasing temperatures. The difference between R_{hs} and R_c, on the other hand, remains basically unaffected by the temperature. According to the values given in Figures 8 and 9, we find R_{hs}-R_c of magnitude 18, 24, and 30 Å for respectively P85, F87, and F88 micelles. In our simplified picture, this difference in radii is the thickness of the PEO shell.

The solutions of P85, F87, and F88 all show very similar temperature and concentration dependencies. It appears that when R_c is plotted against the reduced temperature T-T_{cm1}, the data follow a common master curve. Figure 10 shows in a double-logarithmic plot R_c versus T-T_{cm1}, giving the empirical scaling relation:

$$R_c \propto (T - T_{cm1})^{0.2} \tag{7}$$

It was shown in ref 3 that, to a very good approximation, the micellar core can be considered as consisting of completely dehydrated propylene oxide units, covered by a single monolayer of ethylene oxide. In a numerical study Linse and Malmsten have shown somewhat similar behavior, although they also found that some EO is present inside the core and that some PO monomers are present in the corona.[9] Neglecting the single EO layer, which is anyway small compared to R_c, we then find that to a good approximation the aggregation number scales linearly with the third power of the core radius, R_c:

$$NnV_P = \frac{4}{3}\pi R_c^3 \tag{8}$$

Close to T_{cm1} the aggregation number is therefore very small (close to unity) and increases continuously following a $N \propto (T\text{-}T_{cm1})^{0.6}$ relationship to approximately $N \sim 200$ at the highest temperatures, where spherical micellar aggregates are present.

The cubic gel state of P85 is only stable over a limited temperature regime. In ref 3 we argued that the melting of the cubic lattice close to 60 °C is induced by an abrupt change in the internal micellar structure which passes from a spherical form to prolate ellipsoidal, or rodlike structure. Similar changes in the micellar form are observed for P85 in the low concentration regime. It was stated in ref 3 that near this transition temperature the length of the PPO polymers passing through the micellar center approaches an average value of only 2.5 Å per PO monomer; i.e., the PPO chains must be extended to the maximum. It was speculated that this entropically unfavorable conformation is the main driving force for the spherical-to-rod transformation in the micellar form and thereby the origin of the observed melting of the cubic gel state as well.

From the hard-sphere data analysis, it appears that the main difference between P85, F87, and F88 block copolymer micelles at a given temperature is the size of the micelles. The larger the degree of PEO polymerization m, the smaller the core and thereby the micellar aggregation number, at a given temperature. As it appears from Figure 10, on the other hand, the three types of copolymer micelles have the same core size at the reduced temperature T-T_{cm1}. According to the model in which the micellar stability is limited by a maximum core diameter determined by the length of a fully stretched PPO chain (i.e., of the magnitude of 100 Å for the present polymers), F87 and F88 consequently form stable spherical micelles up to temperatures much beyond that of P85. Structural studies on shear-aligned F87 crystals show melting of the cubic lattice at $T = 68$ °C for a 26% copolymer solution. Viscosity measurements confirm[14] that the cubic phase of F87 is stable up to temperatures on the order of 70–80 °C and show that in F88 it is stable up to at least 90 °C. This is in good agreement with the R_c values shown in Figure 10.

We amplify this discussion further in an attempt to deduce more about L81 solutions. Figure 11 shows the micellar core radius for P85, F87, and F88 obtained at 20 °C, and 50 °C, plotted versus the PEO polymerization degree m. Extrapolating the data from P85, F87, and F88 to the $m = 6$ value for L81, we predict that the R_c value for L81 approaches or exceeds the maximum value given by the length of a fully extended PPO chain. This is probably the reason why L81 does not form spherical

micellar aggregates. The correlation peak observed in a small region of the L81 phase diagram, is however at a q value of the same magnitude as the correlation peak value of P85, F87, and F88, indicating that L81 in some cases also forms aggregates with phase-separated PEO and PPO. Although the spherical hard-sphere analysis is not correct for L81, for comparison purposes we have also made this analysis on L81 within a restricted q range, neglecting the low-q tail (Figure 1). The resulting parameters are $R_c \sim 55$ Å and $R_{hs} \sim 80$ Å.

Dynamic light scattering measurements were made on F87 and F88 at a weight concentration of 2% in the temperature range 40–90 °C. Over this range, the scattered intensity showed only a small increase. (This is not the case with P85, however, which also showed a strong increase in the total (VV) scattered intensity with increasing temperature.) The apparent hydrodynamic radius (R_h), evaluated from the Stokes–Einstein equation using the solvent viscosity, was approximately constant in each case and gave average values of 69 (F87) and 82 Å (F88). These values of R_h agree well with those for R_{hs} obtained by fitting the SANS to eq 4 and shown in Figure 9. Moreover, the weaker sensitivity of R_h to temperature above about 50 °C is also observed for R_{hs} (and R_c).

Depolarized and polarized dynamic light scattering measurements were also made as a function of scattering angle and will be reported in detail elsewhere. Neither F87 nor F88 at a concentration of 2% showed significant depolarized scattering intensity between 40 and 90 °C. With P85 at a concentration of 1% at and above 70 °C there was measurable depolarized scattering revealing significant anisotropy in the scatterers. Extrapolation of the measured relaxation rate in the HV geometry (Γ_{HV}) to zero scattering vector, q, according to the relationship

$$\Gamma_{HV} = q^2D + 6D_R \tag{9}$$

where D is the translational diffusion coefficient, allows evaluation of the rotational diffusion coefficient, D_R. Taking as a first approximation the half-thickness of the rodlike micelle (R_r) to equal the hydrodynamic radius of the spherical micelle which exists at lower temperatures (80 Å for P85),[8] one may estimate the micellar rod length, L, using Broersma's equation for rotational diffusion[26]

$$D_R = [3k_BT/(2\pi\eta L^3)]F(\rho) \tag{10}$$

with $\rho = L/2R_r$.

$$F(\rho) = 2[\ln(2\rho) - 1.45 + 7.5(1(\ln(2\rho) - 0.27)^2)] \tag{11}$$

This gives $L = 1470$ Å at 70 °C increasing to $L = 1680$ Å at 80 °C. These values of L were substantiated by inserting them into the expression of Doi and Edwards for the transational diffusion coefficient:[27]

$$D = \ln(\rho)\, k_BT/[6\pi\eta(L/2)] \tag{12}$$

The value of D was found to be identical within experimental error to the translational diffusion coefficient measured on the same solution in the VV geometry at the same angle and temperature. Similar measurements on P85 at C = 5% gave a rod length of the same magnitude, indicating that, as was observed within the regime of spherical micelles, there is also no significant micellar growth with increasing concentration in the regime of rodlike micelles. At even higher concentration, however, the VV autocorrelation function becomes bimodal, reflecting significant intermicellar correlations, which subsequently result in the crystalline phase of hexagonally ordered rods.[2]

At higher concentration of F88 (C = 20%) at temperatures above 80 °C, the solutions are "stringy" in consistency and the autocorrelation function (VV) is then bimodal, containing a very slowly decaying component. This suggests that micellar growth into rodlike micelles also occurs as with P85 but that aggregates of highly entangled rods are then formed. The above results are consistent with the observed changes in the SANS scattering function for P85 solutions above approximately 60 °C and also that such changes are much less pronounced (F87) or absent (F88) up to at least 90 °C.

IV. Conclusions

The data analysis used to treat the experimental neutron scattering functions is based on a relatively simple model of hard-sphere interacting micelles, in which a dense core of PPO totally dominates the scattering form factor. One may argue that this model is too simple to describe details of the aggregates. Certainly, the resulting micellar parameters may be affected by small systematic errors, and thus the exact numbers coming out of the analysis should be taken with some caution. For example, the effective core radius should possibly be renormalized somewhat before it is used to calculate the aggregation number. As was shown in ref 3, however, we have evidence that this renormalization is small relative to the value of R_c. The presented data analysis gives, on the basis of a simple physical picture, a good understanding of the copolymer aggregates.

We have, in conclusion, shown that a series of block copolymers of the PEO–PPO–PEO type to a large extent follows common rules for phase behavior. In the low-temperature, low-concentration corner of the T–C phase diagram, the copolymers are dissolved as independent unimers. Above a critical micellation temperature $T_{cm1}(C_P)$, micelles starts to form, and basically all copolymers are incorporated into micelles above a second characteristic temperature T_{cm2}. The critical micellization temperature T_{cm1} is, to a good approximation, determined only by the PPO concentration, independent of the PEO chains. Upon increasing the temperature above $T_{cm1}(C_P)$, the micellar aggregates become still larger, until the micellar core diameter at a third characteristic temperature T_{cm3} approaches the size of a fully stretched PPO chain. The micellar structure changes and then abruptly departs from a spherical form. For the P85, F87, and F88 micellar suspensions, the temperature-dependent micellar core size, and thereby aggregation number, all have the same temperature dependence. The much more hydrophobic nature of the L81 copolymers, on the other hand, prevents micelle formation at any temperature. Already at relative low temperature, extrapolation from data for the three other copolymers, P85, F87, and F88, predicts a micellar core diameter of L81 which approaches the length of a fully stretched PPO chain. L81 actually forms large aggregates at temperatures below the critical value expected for micelle formation.

In the high-concentration suspensions of spherical micelles, hard-sphere crystallization is observed for the three systems. The crystalline gel phase is to a good approximation determined by the total polymer concentration.

Acknowledgment. We thank S. Hvidt (Roskilde University) and J. S. Pedersen (Risø National Laboratory) for fruitful discussions. Financial support from the Danish and the Swedish Natural Science Research Councils is gratefully acknowledged.

References and Notes

(1) Mortensen, K.; Brown, W.; Nordén, B. *Phys. Rev. Lett.* **1992**, *68*, 2340–2343.
(2) Mortensen, K. *Europhys. Lett.* **1992**, *19*, 599–604.
(3) Mortensen, K.; Pedersen, J. S. *Macromolecules* **1993**, *26*, 805–812.
(4) Rassing, J.; Attwood, D. *Int. J. Pharm.* **1983**, *13*, 47–55.
(5) Zhou, Z.; Chu, B. *Macromolecules* **1987**, *20*, 3089–3091.
(6) Zhou, Z.; Chu, B. *J. Colloid. Interface Sci.* **1988**, *126*, 171–180.
(7) Wanka, G.; Hoffmann, H.; Ulbricht, W. *Colloid Polym. Sci.* **1990**, *268*, 101–117.
(8) Brown, W.; Schillén, K.; Almgren, M.; Hvidt, S.; Bahadur, P. *J. Phys. Chem.* **1991**, *95*, 1850–1858.
(9) Linse, P.; Malmsten, M. *Macromolecules* **1992**, *25*, 5434–5439.
(10) Yu, G.-E.; Deng, Y.; Dalton, S.; Wang, Q.-G.; Attwood, D.; Booth, C. *J. Chem. Soc., Faraday Trans.* **1992**, *88*, 2537–2544.
(11) Vadnere, M.; Amidon, G. L.; Lindenbaum, S.; Haslam, J. L. *Int. J. Pharm.* **1984**, *22*, 207–218.
(12) Mortensen, K. *Prog. Colloid Polym. Sci.* **1993**, *91*, 69–71.
(13) Mortensen, K. *Prog. Colloid Polym. Sci.* **1993**, *93*, in press.
(14) Brown, W.; Schillén, K.; Hvidt, S. *J. Phys. Chem.* **1992**, *96*, 6038–6044.
(15) Robbins, M. O.; Kremer, K.; Grest, G. S. *J. Chem. Phys.* **1988**, *88*, 3286–3312.
(16) The molecular specification of the P85 $E_mP_nE_m$ triblock copolymer has been reported with different values of m and n, both $m = 25$, $n = 40$ and $m = 27$, $n = 39$. This difference is within the uncertainty of the experimental results and does not influence our conclusions.
(17) Pedersen, J. S.; Posselt, D.; Mortensen, K. *J. Appl. Crystallogr.* **1990**, *23*, 321–333.
(18) Smit, B.; Hilbers, P. A. J.; Esselink, K.; Rupert, L. A. M.; van Os, N. M.; Schlijper, A. G. *Nature* **1990**, *348*, 624–625.
(19) Guinier, A.; Fournet, G. *Small Angle Scattering of X-Rays*; Wiley: New York, 1955.
(20) Percus, J. K.; Yevick, G. J. *Phys. Rev.* **1958**, *110*, 1–13.
(21) Ashcroft, N. W.; Lekner, J. *Phys. Rev.* **1966**, *145*, 83–90.
(22) Kinning, D. J.; Thomas, E. L. *Macromolecules* **1984**, *17*, 1712–1718.
(23) Nicolai, T.; Brown, W.; Johnsen, R. M. *Macromolecules* **1990**, *23*, 1165–1174.
(24) Jakes, J. *Czech. J. Phys.* **1988**, *38*, 1305–1310.
(25) PPO with $M_W = 2000$ have a critical solution temperature of 18 °C for 2% polymer concentration: Mortensen, K.; et al., to be published.
(26) Broersma, S. J. *J. Chem. Phys.* **1960**, *32*, 1626–1632.
(27) Doi, M.; Edwards, S. F. The Theory of Polymer Dynamics; Oxford University Press: Oxford, U.K., 1986, pp 289–323.